Comparison of Experiments and Simulation of Joule Heating in ac Electrokinetic Chips

Stuart J. Williams
Department of Mechanical Engineering,
University of Louisville,
Louisville, KY 40292
e-mail: stuart.williams@louisville.edu

Pramod Chamarthy
General Electric,
Niskayuna, NY 12309
e-mail: pramodchamarthy@yahoo.com

Steven T. Wereley
Mechanical Engineering,
Purdue University,
West Lafayette, IN 47907
e-mail: wereley@purdue.edu

ac electrokinetic manipulations of particles and fluids are important techniques in the development of lab-on-a-chip technologies. Most of these systems involve planar microelectrode geometries, generating high strength electric fields. When these fields are applied to a dielectric medium, Joule heating occurs. Understanding electrothermal heating and monitoring the temperature in these environments are critical for temperature-sensitive investigations including biological applications. Additionally, significant changes in fluid temperature when subjected to an electric field will induce electrohydrodynamic flows, potentially disrupting the intended microfluidic profile. This work investigates heat generated from the interaction of ac electric fields and water at various electrical conductivities (from 0.92 mS/m to 390 mS/m). The electrode geometry is an indium tin oxide (ITO) electrode strip 20 μm wide and a grounded, planar ITO substrate separated by a 50 μm spacer with microfluidic features. Laser-induced fluorescence is used to measure the experimental changes in temperature. A normalization procedure that requires a single temperature-sensitive dye, Rhodamine B (RhB), is used to reduce uncertainty. The experimental electrothermal results are compared with theory and computer simulations. [DOI: 10.1115/1.4000740]

1 Introduction

Micro-electrode structures are used in ac electrokinetics to generate strong electric fields for manipulating suspended micro- and nanoparticles as well as fluids in lab-on-a-chip systems. One such electrokinetic technique, dielectrophoresis (DEP), is used as a noninvasive means to selectively manipulate and capture suspended particles in microfluidic devices [1]. When conductive, electrically neutral particles are subjected to an electric field, they will polarize, inducing applied moments on the particle. If the electric field is nonuniform, there will be an imbalance of moments, resulting in DEP and particle translation. The strength and direction of the DEP forces are dependent on the dielectric properties of the particle and fluid, as well as on the electric field strength. DEP has been used to manipulate micro- and nanometer-sized particles [2,3] as well as DNA [4], viruses [5], and bacteria [6]. ac electroosmosis (ACEO) is another electrokinetic technique referring to the electrokinetic pumping of ionic fluids using ac signals [7,8]. The tangential component of the electric field near the electrode interface acts upon charges in the double layer, resulting in fluid motion. Fluid velocities in the order of mm/s can be achieved with an applied potential of a few V [8].

The strong electric fields necessary for DEP and ACEO are typically generated with fabricated, micrometer-sized electrodes and with an applied ac signal using commercially available benchtop signal generators. Various electrode geometries are used for DEP and ACEO, including interdigitated, comblike structures [6,7,9] for fluid and particle manipulation and single-particle DEP trapping arrangements such as point-and-lid [10], quadruple [11], and octopole [12,13] electrodes. The applied ac signals for DEP and ACEO are typically 0–20 V and frequencies typically between 1 kHz and 10 MHz. The dielectric properties of the fluid medium are dependent on the specific application. Electrical conductivities of the fluid range from deionized (DI) water ($\sim$5.0 μS/m) to biological growth media ($>$1 S/m). DEP experiments incorporating low-conductivity growth media and bacteria have also been reported [14].

These strong electric fields will act on the conducting fluid medium, resulting in Joule heating. This could harm temperature-sensitive biological samples. In addition, the heating changes the conductivity and permittivity of the fluid—the applied electric field will act on these dielectric gradients resulting in electrothermal fluid motion [15–18]. Both Joule heating and electrothermal fluid pumping could be unwanted effects for electrokinetic lab-on-a-chip systems.

It is important to monitor the effects of Joule heating in electrokinetic microsystems. There are a variety of temperature measuring techniques that have been incorporated at this scale [19]. Thermocouples can be incorporated into the microchannel [20] or can be fabricated on the channel surface [21,22]. Similarly, resistance temperature detectors have been used to monitor heat transfer, with their resistive elements fabricated along the microchannel surface [23,24]. Each of these techniques, however, requires precisely controlled fabrication. Thermochromic liquid crystals (TLCs) have also been used for temperature measurements due to their unique, temperature-dependent optical properties. TLC slurries and paints can achieve measurement resolution to approximately 1 μm [25] while encapsulated crystals have been used for simultaneous velocity and temperature measurements [26] as well as transient temperature measurements [27,28]. Infrared thermography has been used to measure the boiling characteristics in microchannels [29,30]. However, infrared thermography can only be used to measure surface temperatures.

Particles exhibit random movement due to their interaction with liquid molecules, a phenomenon called Brownian motion. The suspended particle's displacement due to Brownian motion is proportional to temperature. Both microscale particle tracking and particle image velocimetry thermometry techniques have been adapted in order to measure Brownian motion and determine temperature [31–34]. However, these techniques were not implemented for our experiments as the translation of the tracer particles was affected by DEP and electrokinetic hydrodynamics. Due to these hindrances, an alternate nonintrusive temperature measurement method that did not use tracer particles was chosen.

Contributed by the Fluids Engineering Division of ASME for publication in the JOURNAL OF FLUIDS ENGINEERING. Manuscript received May 27, 2009; final manuscript received October 22, 2009; published online February 4, 2010. Assoc. Editor: Pavlos P. Vlachos.

Among the various methods available, laser-induced fluorescence (LIF) is capable of making nonintrusive temperature measurements within a volume of liquid. For LIF thermometry, the temperature-dependent fluorescent intensity of dyes is utilized to measure temperature. LIF has been used at the microscale previously [35–37]. Two dyes can be used to eliminate uncertainty due to nonuniform illumination [38–40], where the temperature-insensitive dye is used to normalize the intensity of the temperature-sensitive dye. In general, Rhodamine B (RhB) and Rhodamine 110 (Rh110) are used as the temperature-dependent and temperature-independent dyes, respectively. This normalized technique is referred to as the ratiometric laser-induced fluorescence thermometry (R-LIFT) method or the dual emission laser-induced fluorescence (DELIF) method. We have used the R-LIFT method previously for microscale fluid investigations [41]. Here, a normalization procedure that requires a single dye, first used by Ross et al. [37] to measure Joule heating for electroosmotic flow, was applied. What differentiates the present investigation from previous work [37] is the comparison of temperature measurements to numerical simulations for Joule heating in ac electrokinetic chips.

2 Electrothermal Theory

In order to estimate the temperature rise due to Joule heating the energy balance equation needs to be solved [17,18] as follows:

$$\rho_m c_p(\partial T/\partial t + (v \cdot \nabla)T) = k\nabla^2 T + \langle \sigma |\boldsymbol{E}|^2 \rangle + Q \tag{1}$$

where ρ_m is mass density, c_p is the heat capacity, T is temperature, v is velocity, k is thermal conductivity, σ is the electrical conductivity of the liquid, E is the electric field, and Q is a heat source. This equation can be simplified for ac electrokinetic microsystems. The applied ac electric field produces an oscillating temperature component. Scaling analysis by Ramos et al. [17] demonstrated that for a characteristic length scale of 20 μm (the width of electrodes used herein) thermal equilibrium is established within 1 ms of applying the electric field. Therefore, the oscillating temperature component can be neglected for frequencies greater than 1 kHz. Heat convection is negligible when compared with heat conduction as shown with a dimensional analysis of the second term in Eq. (1),

$$|\rho_m c_p (v \cdot \nabla)T|/|k\nabla^2 T| \approx \rho_m c_p v l/k \leq 0.07 \tag{2}$$

where l is the characteristic length of the system ($l < 100$ μm) and the variables are $c_p = 4.18 \times 10^3$ J kg^{-1} K^{-1}, $k = 0.6$ J m^{-1} s^{-1} K^{-1}, $\rho_m = 1000$ kg m^{-3}, and $v < 100$ μm/s [17,18]. This ratio of convective to conductive heat transfer is a form of the Nusselt number. Further, if we assume that the electric field is the only source of generated heat ($Q=0$), then Eq. (1) simplifies to

$$k\nabla^2 T + \langle \sigma |\boldsymbol{E}|^2 \rangle = 0 \tag{3}$$

This equation is used in numerical models to calculate Joule heating for the microsystem.

A similar nondimensional analysis can be applied to the above expression [17],

$$k\Delta T/l^2 \approx \sigma V_{\text{rms}}^2/l^2 \rightarrow \Delta T \approx \sigma V_{\text{rms}}^2/k \tag{4}$$

The above analysis shows that the change in temperature is proportional to the conductivity of the fluid medium (σ) and proportional to voltage squared (V^2). These electrothermal trends will be compared with the results from numerical simulations and experiments.

3 Theory of LIF Thermometry

For laser-induced fluorescence, the dependence of fluorescence radiation I_f on the concentration of the dye C can be expressed with

$$I_f = \beta_c \phi I_0 (1 - e^{-\varepsilon b C}) \tag{5}$$

where β_c, ϕ, I_0, ε, and b are the collection efficiency, quantum efficiency, incident irradiation, molar absorptivity, and absorption path length, respectively. Equation (5) can be simplified at low concentrations of the dye, when less than 5% of the incident irradiation is absorbed,

$$I_f = \beta_c \phi I_0 \varepsilon b C \tag{6}$$

Factors such as photobleaching, nonuniform illumination, nonuniform dye concentration, and fluctuations of light can all affect LIF measurements. Uncertainty due to illumination variations can be minimized using the two-color LIF method and ratiometric normalization methods. Typically RhB is the temperature-sensitive dye and Rh110 is the temperature-insensitive dye. However, Rh110 is, in fact, temperature-dependent ($\sim$0.1% K^{-1}), just not as strongly as RhB ($\sim$2.0% K^{-1}) [39]. The ratio of their fluorescent intensities can be written as

$$I_{\text{RhB}}/I_{\text{Rh110}} = \frac{\beta_{\text{CRhB}} \phi_{\text{RhB}} \varepsilon_{\text{RhB}} C_{\text{RhB}}}{\beta_{\text{CRh110}} \phi_{\text{Rh110}} \varepsilon_{\text{Rh110}} C_{\text{Rh110}}} \tag{7}$$

This expression is independent of incident irradiation (I_0) and absorption path length (b). The absorption spectral intensity ratio and the molar absorptivity ratio are nearly temperature-independent while the quantum efficiency ratio depends on temperature. If the fluorescence of the dyes does not depend on the pH of the solution, then this intensity ratio is only dependent on temperature for a fixed concentration ratio [42]. Proper R-LIFT measurements require careful calibration to correlate the fluorescence intensity ratio of the dyes to the temperature of the fluid.

The calculated normalized image $I_{\text{NR-LIFT}}$ for the R-LIFT can be expressed as

$$I_{\text{NR-LIFT}} = \frac{I_{\text{RhB}}/I_{\text{Rh110}}}{I_{0\text{–RhB}}/I_{0\text{–Rh110}}} \tag{8}$$

where $I_{0\text{–Rhb}}$ and $I_{0\text{–Rh110}}$ denote images for the two dyes at the reference temperature, and I_{Rhb} and I_{Rh110} are images for the two dyes at the measurement temperature. Assuming Rh110 is temperature-independent the image at the reference temperature $I_{0\text{–Rh100}}$ will be identical with the image at the measurement temperature I_{Rh100}. Equation (8) can be simplified to

$$I_{\text{N-LIFT}} = I_{\text{RhB}}/I_{0\text{–RhB}} \tag{9}$$

where a single image for the temperature-dependent dye at a reference temperature can be used to account for the nonuniform illumination as well as the normalization process. This normalization process, first utilized by Ross et al. [37], will be called N-LIFT to differentiate it from the NR-LIFT method. Since a single reference image is sufficient for all measurements, this method can be used to make instantaneous measurements with a single camera. The measurement region in the reference image needs to be identical to that in the measurement region. Also, if the optical path length changes during the experiment, this method cannot be used. The N-LIFT method is used here to determine the temperature of the fluid in a microsystem due to Joule heating in an ac electrokinetic chip.

4 Experimental

Experiments were conducted in a standard microparticle image velocimetry (μPIV) setup, as illustrated in Fig. 1. It consists of an upright microscope (Nikon Eclipse, ME600), an interline transfer charge coupled device (CCD) camera (Roper Scientific Photometrics, CoolSNAP HQ), and a Nikon mercury-arc lamp was used as the illumination source. Images were acquired with METAMORPH imaging software. Laser grade RhB (Acros Organics, Geel, Belgium) was dissolved in different conductivities of water. The dye was mixed in 1 ml of methanol beforehand to increase its solubility in water. The fluid samples were further prepared by dissolving

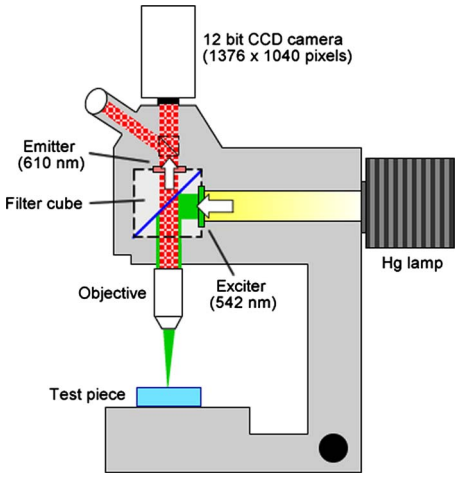

Fig. 1 LIF thermometry experimental setup

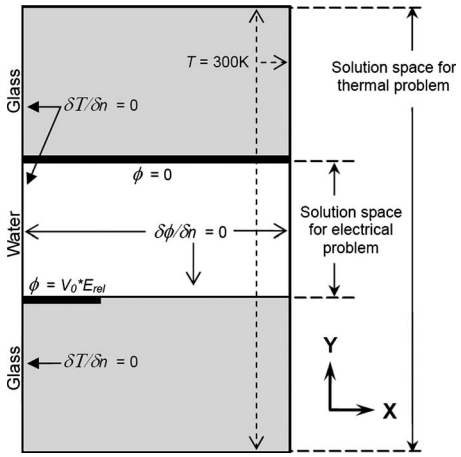

Fig. 3 Schematic of the electrical and thermal problem space and boundary conditions for the numerical model

different amounts of sodium chloride (NaCl) to change its electrical conductivity. Five samples were prepared (one without NaCl) and their conductivity was measured with a bench-top conductivity meter (Denver Instruments, Model 220). The RhB dye was excited with a filter ($\lambda \sim 542$ nm) attached to the front of the mercury-arc lamp.

The calibration experiments were conducted in a 400 μm square glass microchannel (Vitrocom, Inc., Mountain Lakes, NJ) submerged in a well machined from an aluminum block. The capillary was filled with the dye solution, sealed on both ends, and placed in the well. DI water filled the well and was sealed on top with an acrylic plate. The aluminum block was heated using a thermofoil resistance heater (Minco Products, Inc., Minneapolis, MN) and was enclosed in an insulating material. The temperature of the water bath (24–68°C) was measured with a thermal couple at temperature intervals of 2°C. The setup reached equilibrium temperature in approximately 10–15 min, at which the thermocouple showed a steady temperature reading.

The test chip is illustrated in Fig. 2. The top substrate is a transparent, electrically conductive indium tin oxide (ITO) coated glass substrate (0.71 mm thick) with fluidic ports manually drilled. The opposite substrate consists of four independently addressable ITO micro-electrode strips 20 μm wide, 3 mm long, and spaced by 20 μm. These ITO microband chips were commercially available (ABTECH Scientific Inc., Richmond, VA). The sheet resistance (R_s) of the ITO was specified by the manufacturer to be 10 Ω/sq. A microchannel was cut into a double-sided adhesive tape (Adhesives Research Inc., Glen Rock, PA) and provided a 50 μm spacer between the ITO substrates. The microchannel was approximately 1 mm wide and ran perpendicular to the length of the electrode strips. An ac signal (0–25 V_{pp}, 1.0 MHz) was applied across one electrode strip to a grounded ITO plane. The applied frequency of 1.0 MHz was chosen to prevent electrolysis that might otherwise have occurred at lower frequencies for our experiments [18].

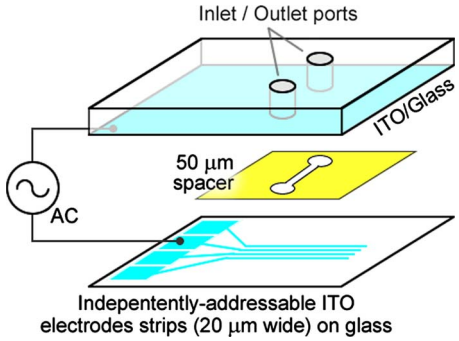

Fig. 2 ac electrokinetic chip for N-LIFT experiments

The temperature of the fluid medium was measured using a thermocouple and this value was used as the reference temperature. The fluid was manually injected into the chip and then adjusted until no bulk fluid motion was observed. At this time a reference temperature image ($I_{0-\mathrm{RhB}}$) was acquired. An ac signal was applied and, after a 1 min delay, five images were acquired within a 1 s time period. The fluorescent intensity of these images was averaged for a single temperature image (I_{RhB}). The signal was turned off and fresh solution was injected for the next trial. This process was repeated for each fluid conductivity sample ($\sigma = 0.918, 104, 200, 319, 390$ mS/m) and each applied voltage ($V_0 = 5, 10, 15, 20, 25$ V_{pp}).

5 Numerical Model

COMSOL MULTIPHYSICS was used for numerical modeling of the electrokinetic chip and simulate Joule heating. The problem space and boundary conditions for the electrical and thermal problems are modeled similarly to the work by Green et al. [16], and is shown schematically in Fig. 3. The thickness of the glass layers is 0.71 mm and fluid-filled spacing is 50 μm. Due to symmetry, the simulation is half of the electrokinetic chip, with only 10 μm of the electrode strip used. The width (x-direction) of the simulation space is extended until minimal changes in the numerical results were noticed (>1.0 mm).

The thermal and electrical problems are decoupled since induced fluid convection does not contribute to the thermal problem. The electrical problem is bounded to within the fluid medium. The Laplace equation for a potential (ϕ) in a homogeneous medium is first solved with [16]

$$\nabla^2 \phi = 0, \quad \boldsymbol{E} = -\nabla \phi \tag{10}$$

The boundary condition for the electrode strip V_0 refers to the rms value of the applied potential.

The ITO traces of the experimental chip cause a loss in the applied electric field. Electrical resistance of the ITO will reduce the applied potential (V_o) by a factor (E_{rel}). The geometry of the independently addressable ITO electrodes was incorporated into a computer model to determine this loss. This model included the ITO-coated glass and the liquid medium between the substrates.

For medium conductivities 0.918 mS/m, 104 mS/m, 200 mS/m, 319 mS/m, 390 mS/m, and 1 S/m, the calculated values of E_{rel} were 0.99, 0.92, 0.86, 0.81, 0.78, and 0.64, respectively. E_{rel} decreased with increasing fluid conductivity. This trend was ex-

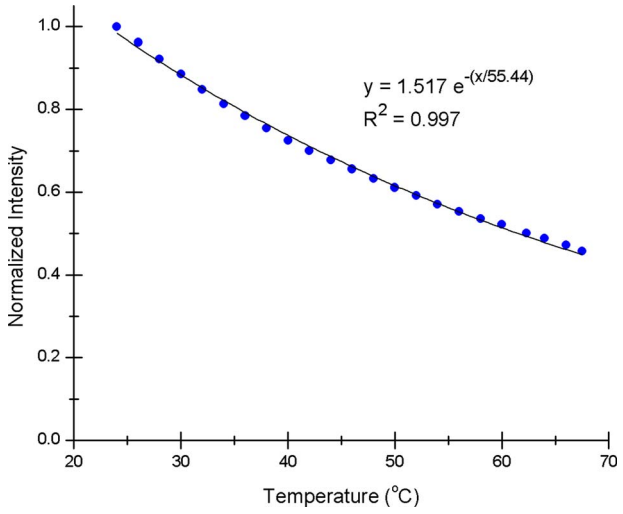

Fig. 4 Normalized fluorescence intensity for RhB

pected as the resistance across the medium decreases with larger fluid conductivities, resulting in a reduced value of the potential applied across the liquid. From Eq. (4) it is expected that the increase in temperature is proportional to the conductivity of the fluid; however, incorporation of E_{rel} will result in a nonlinear relationship. The manufactured ITO had a sheet resistance of 10 Ω/sq; if gold or a more conductive material was used for the electrodes there would be less electrical loss, leading to increased E_{rel} values.

The applied voltage in the numerical model was multiplied by this factor ($\phi = E_{rel} V_0$). After solving for the electric field, this value was used to solve the thermal problem in Eq. (3) with the values of the thermal conductivity (k) of water and glass being set at 0.6 J m^{-1} s^{-1} K^{-1} and 1.0 J m^{-1} s^{-1} K^{-1}, respectively.

6 Results and Discussion

The fluorescent intensity of the calibration images was normalized with the image acquired at room temperature (24°C, arbitrarily chosen) and shown in Fig. 4. The calibration data were

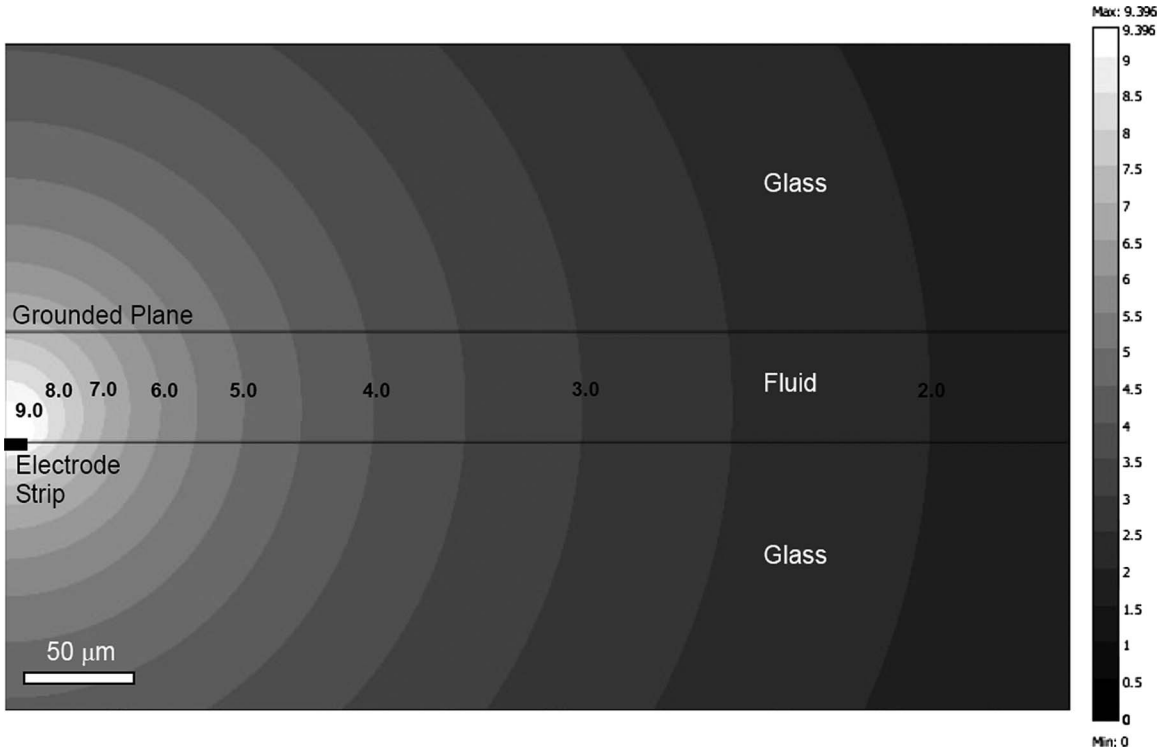

Fig. 5 A portion of the numerical simulation showing the increase in temperature due to Joule heating for a fluid sample with conductivity $\sigma = 200$ mS/m and applied voltage $V = 20$ V_{pp}

Table 1 Maximum temperature change from numerical simulations and experiments

Conductivity (mS/m)	Change in temperature									
	Simulations ($T_0 = 300$ K)					Experiment				
	Applied voltage (V_{pp})					Applied voltage (V_{pp})				
	5	10	15	20	25	5	10	15	20	25
0.918[a]	0.004	0.015	0.035	0.061	0.096	0.3	−0.4	−0.5	3.3	0.8
104	0.37	1.47	3.31	5.89	9.20	0.4	2.2	4.3	6.1	10.5
200	0.62	2.49	5.61	9.97	15.57	1.1	1.3	4.6	9.6	14.1
319	0.87	3.47	7.82	13.9	21.7	0.3	2.3	6.4	12.1	19.7
390	0.99	3.97	8.93	15.9	24.8	1.8	3.9	10.0	17.2	26.6
1000	1.70	6.81	15.3	27.2	42.6					

[a]No NaCl was added to the RhB solution.

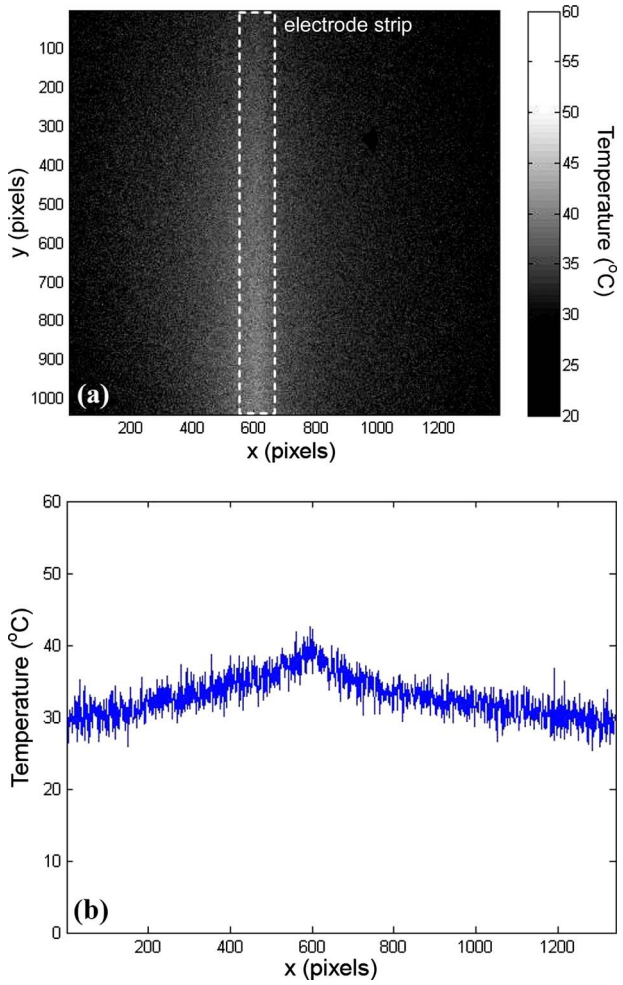

Fig. 6 (*a*) N-LIFT results showing the temperature increase in the medium (σ=200 mS/m) above the electrode strip at 25 V_{pp}. (*b*) Averaged temperature values across the strip.

fitted to an exponential decay, and this curve was used to determine the measured temperature from acquired images.

Numerical simulations were conducted for each of the five experimental fluid conductivities and five applied voltages. A zoomed-in plot for one of the simulations (200 mS/m, 20 V_{pp}) is shown in Fig. 5. The maximum temperature increase occurs at the interface of the electrode strip. The maximum value for the temperature increase from numerical simulations was recorded and compared with the maximum value obtained from experimental measurements (Table 1).

Figure 6(*a*) shows a normalized image obtained from N-LIFT (top-view) with the electrode strip running vertically along the length of the image for σ=200 mS/m and V=25 V_{pp}. The temperature values perpendicular to the electrode strip were averaged, Figure 6(*b*) shows the resulting temperature profile. The maximum temperature increase was recorded and compared with numerical simulations (Table 1).

Table 1 shows the maximum temperature change from both numerical simulations and experiments. To illustrate the Joule heating trends of these obtained values, Fig. 7 shows the temperature increase plotted against voltage squared (V_{pp}^2) for each conductivity, and Fig. 8 has temperature increase versus medium conductivity. Experimental measurements are shown with points while numerical simulation values are shown with a solid line and labeled with parentheses.

The experimental data follow the expected trend that temperature is proportional to the square of the applied voltage (V^2).

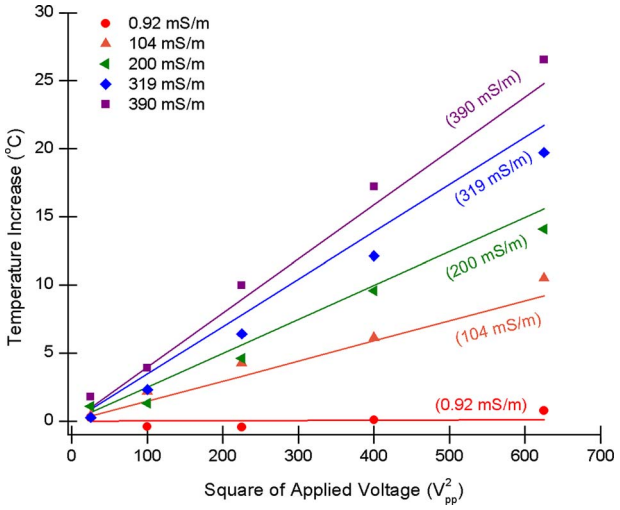

Fig. 7 Obtained maximum change in temperature values versus voltage squared obtained from N-LIFT experiments (data points) and numerical simulations (lines)

Theory also states that temperature change is proportional to fluid conductivity; however, the resulting curve (Fig. 8) is nonlinear due to the loss of the applied field to the ITO traces. The loss in electric field increased with greater fluid conductivity. Joule heating is negligible for the fluid sample with conductivity 0.918 mS/m, and trends could not be identified with LIF thermometry. In addition, simulations calculated the expected increase in temperature for this low conductive solution at 25 V_{pp} was less than 0.1°C. The maximum measured temperature change of 26.6°C occurred with the 390 mS/m fluid sample at 25 V_{pp}. However, typical biological growth media have conductivities greater than 1 S/m. For example, phosphate-buffered saline (PBS) and Dulbecco's modified eagle medium (DMEM) each have an electrical conductivity greater than 1 S/m [43]. Numerical simulations calculated a temperature increase of almost 1.7°C for a 1 S/m sample at 5 V_{pp} and over 42°C at 25 V_{pp} (Table 1). Therefore any temperature-sensitive electrokinetic microsystem with biological growth media or other high-conductivity fluid needs to be carefully monitored for Joule heating.

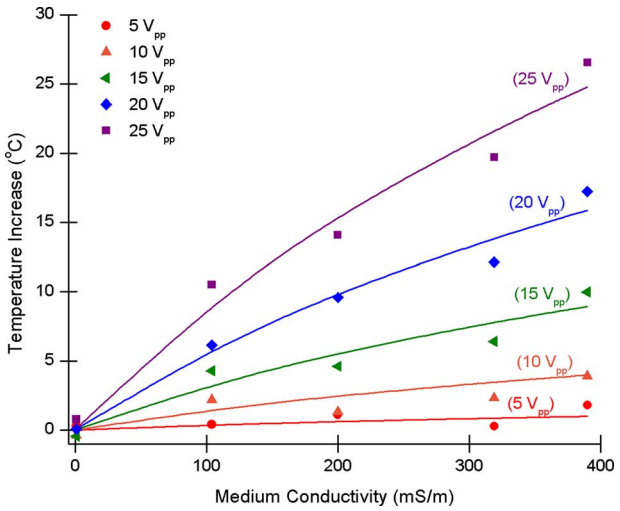

Fig. 8 Obtained maximum change in temperature values versus conductivity obtained from N-LIFT experimental measurements (data points) and numerical simulations (lines)

Electrokinetically induced fluid flow was readily observed visually for all but the least conductive fluid sample with applied voltages of 20 V_{pp} and 25 V_{pp}. This fluid flow is a combination of electrothermal hydrodynamics and ACEO. Microfluidic measurement techniques such as μPIV could be utilized to quantify and characterize this electrokinetic fluid velocity. The aim of future experiments will investigate the impact of Joule heating on electrokinetically induced flow. This flow can disrupt any intended fluid flow in microfluidic systems, especially at high applied voltages.

The thermal noise present in the camera and the uncertainty involved in the calibration curve are the two main sources of error in this technique. The uncertainty involved in the calibration curve represents the accuracy of the method while the thermal noise represents the variation in the measurements. The error involved in the measurement of temperature e_T can be expressed as

$$e_T = \pm \{(e_C)^2 + (e_N)^2\}^{1/2} \tag{11}$$

where e_C is the error involved in the calibration curve and e_N is error due to thermal noise. The error due to the thermal noise e_N, defined as the standard deviation of the single-pixel measurement, was $\pm 1.1\,^{\circ}$C for the N-LIFT method. The uncertainty involved in the calibration curve depends on the difference between the normalization temperature and the measured temperature increases. The mean uncertainty involved in the calibration curve e_C was measured to be $\pm 0.6\,^{\circ}$C. The total error in the measurement of temperature was estimated to be $\pm 1.25\,^{\circ}$C for the N-LIFT method. This uncertainty is less than measurements with a similar, two-color normalization method (NR-LIFT) under similar experimental conditions. Additional error is introduced with the NR-LIFT method from single-pixel measurements of both dyes, as opposed to one dye in the method described herein. In addition, Rh110 is slightly temperature-dependent ($\sim 0.2\%/\,^{\circ}$C), introducing additional error, especially at higher temperatures. Therefore, the N-LIFT method has less uncertainty than the NR-LIFT method. However, one drawback is the introduction of uncertainties when comparing the acquired image to only one reference image at a known temperature, especially at measured temperatures much greater than the reference temperature.

These uncertainties are for single-pixel measurements. The error due to the thermal noise can be reduced by averaging over larger areas. For the recorded temperatures (Table 1), e_N can be effectively neglected as it was averaged over a large number of pixels. Hence, the uncertainty involved in the N-LIFT measurements will be e_C, $\pm 0.6\,^{\circ}$C.

ac electrokinetic techniques such as DEP and ACEO are utilized for lab-on-a-chip microsystems due to their inherently strong electric fields; however, these electric fields heat the fluid sample. Monitoring Joule heating effects is especially important for temperature-sensitive experiments and biological samples. LIF thermometry utilizing the N-LIFT method is a simple procedure to noninvasively measure Joule heating effects. In addition, numerical simulations can assist in designing proper electrokinetic chips to minimize unwanted Joule heating.

7 Conclusions

A LIF normalization procedure that requires a single dye [37] was used to determine Joule heating in a simple ac electrokinetic chip. Fluid samples of various conductivities (0.918 mS/m, 104 mS/m, 200 mS/m, 314 mS/m, and 390 mS/m) were subjected to electric potentials from 5 V_{pp} to 25 V_{pp} at 1 MHz. Numerical simulations were in good agreement with experimental measurements. Further, experimental data verified expected theoretical trends that temperature is proportional to the square of the applied voltage squared (V^2).

Acknowledgment

S.J.W. acknowledges support under a National Science Foundation Graduate Research Fellowship and a Purdue University's Laura Winkelman Fellowship for Doctoral Studies in the School of Mechanical Engineering.

References

[1] Pohl, H. A., 1978, *Dielectrophoresis: The Behavior of Neutral Matter in Nonuniform Electric Fields*, Cambridge University Press, Cambridge.

[2] Müller, T., Gerardino, A., Schnelle, T., Shirley, S. G., Bordoni, F., De Gasperis, G., Leoni, R., and Fuhr, G., 1996, "Trapping of Micrometre and Sub-Micrometre Particles by High-Frequency Electric Fields and Hydrodynamic Forces," J. Phys. D: Appl. Phys., **29**, pp. 340–349.

[3] Schnelle, T., Muller, T., Gradl, G., Shirley, S. G., and Fuhr, G., 2000, "Dielectrophoretic Manipulation of Suspended Submicron Particles," Electrophoresis, **21**, pp. 66–73.

[4] Holzel, R., Gajovic-Eichelmann, N., and Bier, F. F., 2003, "Oriented and Vectorial Immobilization of Linear M13 dsDNA Between Interdigitated Electrodes—Towards Single Molecule DNA Nanostructures," Biosens. Bioelectron., **18**, pp. 555–564.

[5] Morgan, H., Hughes, M. P., and Green, N. G., 1999, "Separation of Submicron Bioparticles by Dielectrophoresis," Biophys. J., **77**, pp. 516–525.

[6] Li, H. B., Zheng, Y. N., Akin, D., and Bashir, R., 2005, "Characterization and Modeling of a Microfluidic Dielectrophoresis Filter for Biological Species," J. Microelectromech. Syst., **14**, pp. 103–112.

[7] Ajdari, A., 2000, "Pumping Liquids Using Asymmetric Electrode Arrays," Phys. Rev. E, **61**, pp. R45–R48.

[8] Studer, V., Pepin, A., Chen, Y., and Ajdari, A., 2004, "An Integrated AC Electrokinetic Pump in a Microfluidic Loop for Fast and Tunable Flow Control," Analyst (Cambridge, U.K.), **129**, pp. 944–949.

[9] Suehiro, J., and Pethig, R., 1998, "The Dielectrophoretic Movement and Positioning of a Biological Cell Using a Three-Dimensional Grid Electrode System," J. Phys. D: Appl. Phys., **31**, pp. 3298–3305.

[10] Gray, D. S., Tan, J. L., Voldman, J., and Chen, C. S., 2004, "Dielectrophoretic Registration of Living Cells to a Microelectrode Array," Biosens. Bioelectron., **19**, pp. 771–780.

[11] Huang, Y., and Pethig, R., 1991, "Electrode Design for Negative Dielectrophoresis," Meas. Sci. Technol., **2**, pp. 1142–1146.

[12] Schnelle, T., Muller, T., and Fuhr, G., 2000, "Trapping in AC Octode Field Cages," J. Electrost., **50**, pp. 17–29.

[13] Schnelle, T., Hagedorn, R., Fuhr, G., Fiedler, S., and Muller, T., 1993, "Three-Dimensional Electric-Field Traps for Manipulation of Cells—Calculation and Experimental-Verification," Biochim. Biophys. Acta, **1157**, pp. 127–140.

[14] Yang, L., Banada, P. P., Bhunia, A. K., and Bashir, R., 2008, "Effects of Dielectrophoresis on Growth, Viability and Immuno-Reactivity of *Listeria Monocytogenes*," Journal of Biological Engineering, 2:6.10.1186/1754-1611-2-6

[15] Green, N. G., Ramos, A., Gonzalez, A., Castellanos, A., and Morgan, H., 2000, "Electric Field Induced Fluid Flow on Microelectrodes: The Effect of Illumination," J. Phys. D: Appl. Phys., **33**, pp. L13–L17.

[16] Green, N. G., Ramos, A., Gonzalez, A., Castellanos, A., and Morgan, H., 2001, "Electrothermally Induced Fluid Flow on Microelectrodes," J. Electrost., **53**, pp. 71–87.

[17] Ramos, A., Morgan, H., Green, N. G., and Castellanos, A., 1998, "Ac Electrokinetics: A Review of Forces in Microelectrode Structures," J. Phys. D: Appl. Phys., **31**, pp. 2338–2353.

[18] Castellanos, A., Ramos, A., Gonzalez, A., Green, N. G., and Morgan, H., 2003, "Electrohydrodynamics and Dielectrophoresis in Microsystems: Scaling Laws," J. Phys. D: Appl. Phys., **36**, pp. 2584–2597.

[19] Jaeger, M. S., Mueller, T., and Schnelle, T., 2007, "Thermometry in Dielectrophoresis Chips for Contact-Free Cell Handling," J. Phys. D: Appl. Phys., **40**, pp. 95–105.

[20] Lee, P. S., Garimella, S. V., and Liu, D., 2005, "Investigation of Heat Transfer in Rectangular Microchannels," Int. J. Heat Mass Transfer, **48**, pp. 1688–1704.

[21] Chen, T. L., and Garimella, S. V., 2006, "Measurements and High-Speed Visualizations of Flow Boiling of a Dielectric Fluid in a Silicon Microchannel Heat Sink," Int. J. Multiphase Flow, **32**, pp. 957–971.

[22] Jang, S. P., Kim, S. J., and Paik, K. W., 2003, "Experimental Investigation of Thermal Characteristics for a Microchannel Heat Sink Subject to an Impinging Jet, Using a Micro-Thermal Sensor Array," Sens. Actuators, A, **105**, pp. 211–224.

[23] Jiang, L. N., Wang, Y. L., Wong, M., and Zohar, Y., 1999, "Fabrication and Characterization of a Microsystem for a Micro-Scale Heat Transfer Study," J. Micromech. Microeng., **9**, pp. 422–428.

[24] Sammarco, T. S., and Burns, M. A., 1999, "Thermocapillary Pumping of Discrete Drops in Microfabricated Analysis Devices," AIChE J., **45**, pp. 350–366.

[25] Höhmann, C., and Stephan, P., 2002, "Microscale Temperature Measurement at an Evaporating Liquid Meniscus," Exp. Therm. Fluid Sci., **26**, pp. 157–162.

[26] Fujisawa, N., Funatani, S., and Katoh, N., 2005, "Scanning Liquid-Crystal Thermometry and Stereo Velocimetry for Simultaneous Three-Dimensional Measurement of Temperature and Velocity Field in a Turbulent Rayleigh-Bérnard Convection," Exp. Fluids, **38**, pp. 291–303.

[27] Nozaki, T., Mochizuki, T., Kaji, N., and Mori, Y. H., 1995, "Application of

Liquid-Crystal Thermometry to Drop Temperature-Measurements," Exp. Fluids, **18**, pp. 137–144.
[28] Richards, C. D., and Richards, R. F., 1998, "Transient Temperature Measurements in a Convectively Cooled Droplet," Exp. Fluids, **25**, pp. 392–400.
[29] Hetsroni, G., Gurevich, M., Mosyak, A., Pogrebnyak, E., Rozenblit, R., and Yarin, L. P., 2003, "Boiling in Capillary Tubes," Int. J. Multiphase Flow, **29**, pp. 1551–1563.
[30] Hetsroni, G., Mosyak, A., and Segal, Z., 2001, "Nonuniform Temperature Distribution in Electronic Devices Cooled by Flow in Parallel Microchannels," IEEE Trans. Compon. Packag. Technol., **24**, pp. 16–23.
[31] Chamarthy, P., Garimella, S. V., and Wereley, S. T., 2009, "Non-Intrusive Temperature Measurement Using Microscale Visualization Techniques," Exp. Fluids, **47**, pp. 159–170.
[32] Hohreiter, V., Wereley, S. T., Olesen, M. G., and Chung, J. N., 2002, "Cross-Correlation Analysis for Temperature Measurement," Meas. Sci. Technol., **13**, pp. 1072–1078.
[33] Olsen, M. G., and Adrian, R. J., 2000, "Brownian Motion and Correlation in Particle Image Velocimetry," Opt. Laser Technol., **32**, pp. 621–627.
[34] Park, J. S., Choi, C. K., and Kihm, K. D., 2005, "Temperature Measurement for Nanoparticle Suspension by Detecting the Brownian Motion Using Optical Serial Sectioning Microscopy (OSSM)," Meas. Sci. Technol., **16**, pp. 1418–1429.
[35] Kim, H. J., and Kihm, K. D., 2002, "Two-Color (Rh-B & Rh-110) Laser Induced Fluorescence (LIF) Thermometry With Sub-Millimeter Measurement Resolution," ASME J. Heat Transfer, **124**, p. 596.
[36] Kim, H. J., Kihm, K. D., and Allen, J. S., 2003, "Examination of Ratiometric Laser Induced Fluorescence Thermometry for Microscale Spatial Measurement Resolution," Int. J. Heat Mass Transfer, **46**, pp. 3967–3974.
[37] Ross, D., Gaitan, M., and Locascio, L. E., 2001, "Temperature Measurement in Microfluidic Systems Using a Temperature-Dependent Fluorescent Dye," Anal. Chem., **73**, pp. 4117–4123.
[38] Coolen, M. C. J., Kieft, R. N., Rindt, C. C. M., and van Steenhoven, A. A., 1999, "Application of 2-D LIF Temperature Measurements in Water Using a Nd: YAG laser," Exp. Fluids, **27**, pp. 420–426.
[39] Sakakibara, J., and Adrian, R. J., 1999, "Whole Field Measurement of Temperature in Water Using Two-Color Laser Induced Fluorescence," Exp. Fluids, **26**, pp. 7–15.
[40] Natrajan, V. K., and Christensen, K. T., 2009, "Two-Color Laser-Induced Fluorescent Thermometry for Microfluidic Systems," Meas. Sci. Technol., **20**, 015401.
[41] Pramod, C., Wereley, S. T., and Garimella, S. V., 2007, "Microscale Laser-Induced Fluorescence Method for Non-Intrusive Temperature Measurement," ASME International Mechanical Engineering Congress and Exposition, Seattle, WA.
[42] Guilbault, G. G., 1973, *Practical Fluorescence; Theory, Methods, and Techniques*, Dekker, New York.
[43] Fuhr, G., Mueller, T., Baukloh, V., and Lucas, K., 1998, "High-Frequency Electric Field Trapping of Individual Human Spermatozoa," Hum. Reprod., **13**, pp. 136–141.